Cell Metabolism
Article

# In Vivo Correction of COX Deficiency by Activation of the AMPK/PGC-1α Axis

Carlo Viscomi,[1,4] Emanuela Bottani,[1,4] Gabriele Civiletto,[1] Raffaele Cerutti,[1] Maurizio Moggio,[2] Gigliola Fagiolari,[2] Eric A. Schon,[3] Costanza Lamperti,[1] and Massimo Zeviani[1,*]
[1]Unit of Molecular Neurogenetics, The Foundation "Carlo Besta" Institute of Neurology–IRCCS, 20126 Milan, Italy
[2]Neuromuscular Unit, Department of Neurology, The Foundation Cà Granda-Ospedale Maggiore-Policlinico and University of Milan–IRCCS, 20122 Milan, Italy
[3]Department of Neurology, College of Physicians and Surgeons, Columbia University, New York, NY 10032, USA
[4]These authors contributed equally to this work
*Correspondence: zeviani@istituto-besta.it
DOI 10.1016/j.cmet.2011.04.011


## SUMMARY

**Increased mitochondrial biogenesis by activation of PPAR- or AMPK/PGC-1α-dependent homeostatic pathways has been proposed as a treatment for mitochondrial disease. We tested this hypothesis on three recombinant mouse models characterized by defective cytochrome *c*-oxidase (COX) activity: a knockout (KO) mouse for *Surf1*, a knockout/knockin mouse for *Sco2*, and a muscle-restricted KO mouse for *Cox15*. First, we demonstrated that double-recombinant animals overexpressing *PGC-1α* in skeletal muscle on a *Surf1* KO background showed robust induction of mitochondrial biogenesis and increase of mitochondrial respiratory chain activities, including COX. No such effect was obtained by treating both *Surf1*$^{-/-}$ and *Cox15*$^{-/-}$ mice with the pan-PPAR agonist bezafibrate, which instead showed adverse effects in either model. Contrariwise, treatment with the AMPK agonist AICAR led to partial correction of COX deficiency in all three models, and, importantly, significant motor improvement up to normal in the *Sco2*$^{KO/KI}$ mouse. These results open new perspectives for therapy of mitochondrial disease.**

## INTRODUCTION

Present in virtually all eukaryotes, mitochondria are the major source of the high-energy phosphate molecule adenosine triphosphate (ATP), which is synthesized by the mitochondrial respiratory chain (MRC) through the process of oxidative phosphorylation (OXPHOS) (Wallace, 2005). ATP is the principal energy substrate required for all active processes within the cell, and ATP deficiency leads to cellular dysfunction and ultimately cell death. A host of pathways and enzymatic functions residing within mitochondria can modify and influence OXPHOS, and OXPHOS abnormalities can in turn generate signals that trigger either homeostatic pathways, e.g., mitochondrial biogenesis, or execution programs, e.g., mitophagy, which eliminates single dysfunctional organelles, or apoptosis, which eliminates the whole dysfunctional cell (Goldman et al., 2010).

A complex, finely tuned homeostatic system senses the dynamic balance between energy demand and expenditure and regulates the biogenesis, activity, and coupling of mitochondria, according to type, function, and metabolic status of cells and tissues (Wallace and Fan, 2010). In mammals, a master regulator of mitochondrial biogenesis is PPAR-gamma Coactivator 1 alpha (PGC-1α), a transcriptional coactivator that is physiologically induced or activated by conditions of shortage of, or increased demand for, energy, such as cold, physical activity and fasting (Handschin and Spiegelman, 2006). PGC-1α acts by interacting with, and increasing the activity of, a number of transcription factors that in turn induce genes directly or indirectly related to mitochondrial proliferation, oxidative catabolism, and respiration. For instance, PGC-1α interacts with, and potentiates the function of, nuclear respiratory factors (NRF1 and NRF2) and α, β/δ, and γ isoforms of the peroxisomal proliferator activated receptors (PPARs). Both NRF1 and NRF2 induce the expression of several nucleus-encoded subunits of MRC complexes, and of genes involved in replication and transcription of mtDNA, including Tfam (Kelly and Scarpulla, 2004). PPARs are tissue-specific, or ubiquitously expressed, nuclear receptors of fatty acids, which act as their activating ligands. The principal action of PPARs is to induce transcription of genes encoding enzymes involved in cellular and organelle uptake of fatty acids and fatty acid oxidation (FAO), in both mitochondria and peroxisomes (Lefebvre et al., 2006; Barish et al., 2006). PGC-1α is activated by posttranslational modifications, including phosphorylation and deacetylation. Phosphorylation at PGC-1α $T_{177}$ and $S_{538}$ residues is operated by the AMP-dependent kinase (AMPK) (Jäger et al., 2007). Again, this activation responds to a physiological homeostatic mechanism, since ATP and AMP are part of the same nucleotide pool, their levels being inversely related, so that when shortage of the former occurs, the latter increases, and vice versa. As a consequence of increased AMP levels, reflecting low ATP availability and low energy reserve, AMPK is activated, resulting in a cascade of phosphorylation-dependent adaptive modifications of several factors, including PGC-1α, that ultimately determine the shutdown of anabolic, energy-consuming processes, whereas catabolic, energy-producing pathways, such as FAO and MRC, are switched on. AMPK activates PGC-1α not only by direct

phosphorylation but also by indirect means, for instance by activating the $NAD^+$-dependent deacetylase sirtuin 1, Sirt1, which in turn increases the amount of deacetylated, active form of PGC-1α (Cantó et al., 2009). Sirt1 activation by AMPK is mainly due to increased $NAD^+$/NADH ratio, a condition that stimulates Sirt1, as a consequence of AMPK-mediated increased expression of FAO (and OXPHOS) genes, and also of the Nampt gene, encoding the enzyme that converts nicotinamide into $NAD^+$ (Cantó et al., 2009). AMPK is a heterotrimer consisting of a catalytic α subunit and two regulatory subunits, β and γ. The latter subunits exist as multiple isoforms, giving 12 different possible combinations of holoenzyme with different tissue distribution and subcellular localization. AMPK is allosterically stimulated by AMP and is itself regulated by phosphorylation via two main upstream AMPK kinases (Cantó and Auwerx, 2010; Steinberg and Kemp, 2009). The major regulatory phosphorylation site of AMPK has been identified as $T_{172}$ within the catalytic loop between the DFG and APE motifs of the α subunit (Fogarty et al., 2010). Besides physiological conditions, PGC-1α and PPARs can also be stimulated or induced pharmacologically. For instance, bezafibrate is a pan-PPAR agonist that is widely used to treat the metabolic syndrome and hyperlipidemias (Tenenbaum et al., 2005). Resveratrol, a natural polyphenol compound, activates PGC-1α via Sirt1 (Lagouge et al., 2006), and 5-aminoimidazole-4-carboxamide ribonucleoside (AICAR) does so by generating inosine monophosphate, which acts as an AMPK agonist by mimicking AMP (Corton et al., 1995; Merrill et al., 1997).

Mitochondrial disorders are clinical entities associated with defects of OXPHOS, which are ultimately genetically determined (Wallace, 2010). Mitochondrial disorders can be determined by mutations in mtDNA, or in OXPHOS-related nuclear genes (Zeviani and Di Donato, 2004). Many pathogenic mtDNA mutations are heteroplasmic, i.e., they coexist with a variable percentage of wild-type mtDNA. Clinical symptoms typically ensue when the amount of mutant mtDNA offsets a critical threshold, usually >50%–60% of total mtDNA, below which the mutation has virtually no clinical impact. Likewise, most of the mitochondrial syndromes due to mutations in nuclear genes behave as recessive traits and in many cases are determined either by mutations in "ancillary" proteins that play an arguably relevant, but nevertheless not essential, often partially redundant, role in OXPHOS, or by hypomorphic mutant alleles encoding a crippled but still partially functional protein. These observations have suggested the hypothesis that the deleterious effects of either mtDNA- or nuclear-gene mutations could be overcome, at least partially, by increasing the total amount of mitochondria and/or of functionally active "MRC units," via activation of the mitochondrial biogenesis program in critical tissues (Bastin et al., 2008; Wenz et al., 2008). This idea has first been tested in cells from mitochondrial disease patients, by overexpressing recombinant *PGC-1α* or by adding bezafibrate in the medium (Bastin et al., 2008; Srivastava et al., 2009). Both treatments showed mutant cells to partially recover MRC activities and increase ATP production. Oral bezafibrate has later been reported to ameliorate the clinical conditions and the biochemical impairment of a *cre*-lox murine model of COX-defective myopathy, determined by muscle-specific ablation of Cox10, the *heme b* farnesyl transferase, by expressing the cre recombinase under the myosin light-chain 1F (MLC1F) promoter. Here, we report the results of experimental treatments carried out on three other mouse models of COX deficiency: (1) a *Surf1* constitutive knockout (KO) mouse, (2) a muscle-specific *Cox15* KO mouse, and (3) a constitutive knockout/knockin *Sco2* mouse ($Sco2^{KO/KI}$) (Yang et al., 2010) carrying a *null Sco2* allele and a second *Sco2* allele with a missense mutation E129K, corresponding to the E140K recurrent, pathogenic change in *SCO2* mutant patients. Absence of Surf1, an assembly factor of COX, causes severe COX deficiency and fatal Leigh syndrome in children, but milder COX deficiency, and hardly any clinical sign, in mice (Dell'Agnello et al., 2007). Mutations in Cox15, the key enzyme for the conversion of *heme o* into *heme a* (Khalimonchuk and Rödel, 2005), lead to fatal encephalocardiomyopathy in children (Antonicka et al., 2003; Bugiani et al., 2005) and severe myopathy with marked COX deficiency in muscle-restricted KO mice (this paper). Sco2 is a metallochaperone involved in copper metallation of COX (Leary et al., 2009), mutations in which lead to infantile fatal encephalocardiomyopathy (Papadopoulou et al., 1999).

## RESULTS

### Overexpression of PGC-1α Increases MRC Activities

We first investigated a transgenic mouse that overexpresses *PGC-1α* under the promoter of the skeletal-muscle-specific creatine-kinase (MCK) gene (*MCK-PGC-1α*). Muscle-restricted overexpression of the *PGC-1α* gene in the transgenic individuals was 10.7 ± 2.9-fold that of controls, resulting in a 4-fold steady-state increase in the amount of the PGC-1α protein (Figure 1A). The *MCK-PGC-1α* mice are vital, with hardly any clinically relevant features; however, they did show a 3- to 4-fold increase in both muscle mtDNA content (from 1900 ± 674 to 6706 ± 394 copies/cell) and citrate synthase (CS) activity in muscle homogenate (from 337.9 ± 48.6 to 948.4 ± 139.3 nmol/min/mg of protein), two indexes of mitochondrial mass, compared to WT littermates (Figures 1B and 1C). We also determined the expression levels of the immediate targets of PGC-1α, i.e., *Nrf1* and *Nrf2*, and of several downstream targets of the latter factors, including *Tfam*, *COI*, *COII*, *COXIV*, and *COX5a* (Figure 1D). The mRNA levels of both *Nrf* genes remained unchanged, whereas the downstream genes were all overexpressed 2- to 3-fold in *MCK-PGC-1α* muscle samples, compared to those of WT littermates. These findings are fully compatible with the role of PGC-1α as a coactivator that increases the transcriptional activity of several factors, including the Nrf's, but is not a transcription factor by itself. Increased expression of COX subunit transcripts was correlated to increased amount of the corresponding proteins, demonstrated by quantitative western blot (WB) immunovisualization (Figure 1A), which resulted in a 1.5- to 2-fold increase in the specific activities of MRC complexes, cI cII, cIII, and cIV (Figure 1C).

PGC-1α is also known to activate factors, e.g., PPARs, that increase the cellular and organelle uptake, and the catabolic oxidation, of fatty acids (FAO). This effect was reflected by a 3.5-fold increased expression in *MCK-PGC-1α* mouse muscle of *CD36/FAT*, a gene encoding the plasma membrane transporter of fatty acids (Figure 1D).

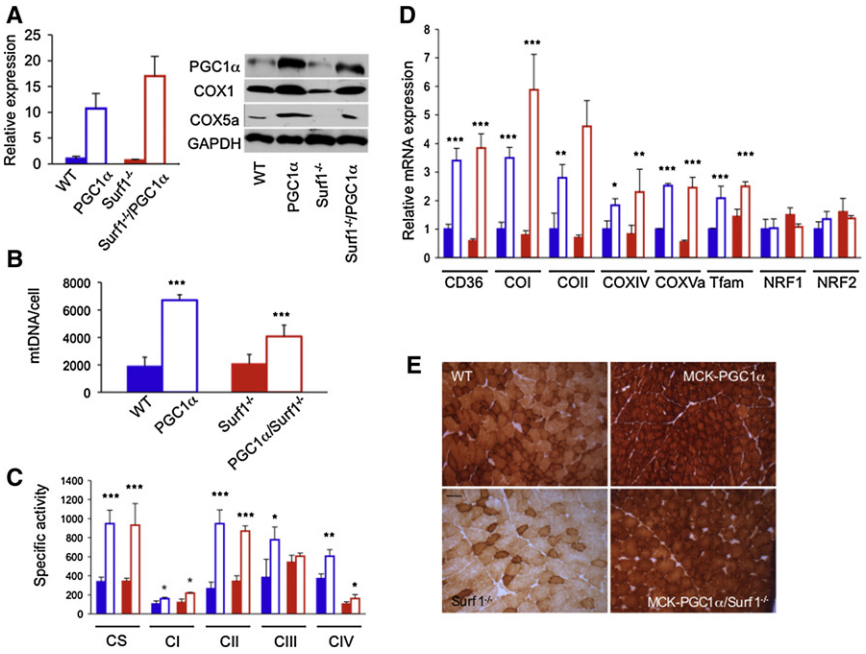


**Figure 1. Effects of *PGC-1α* Overexpression in *Surf1*$^{-/-}$ Mice**

(A) Expression analysis of *PGC-1α*. (Left panel) The *PGC-1α* transcript from muscle of each mouse genotype (three animals/genotype) was retrotranscribed into cDNA, normalized to that of the *Hprt* gene, and expressed as time-fold variations relative to the values obtained from wild-type (WT) animals. Solid blue, WT; blue outline, *PGC-1α*: *MCK-PGC-1α* transgenic mouse; solid red, *Surf1*$^{-/-}$, constitutive *Surf1 knockout* mouse; red outline, *Surf1*$^{-/-}$*/PGC-1α*: *Surf1*$^{-/-}$*/MCK-PGC-1α* double mutant mouse. Error bars represent the standard deviation (SD). (Right panel) Western blot immunovisualization of skeletal muscle proteins of the different genotypes, listed as above. Densitometric analysis of each band, normalized against that of GAPDH, revealed the following variations, relative to WT. (1) PGC-1α, 4.3 in *MCK-PGC-1α*; 0.5 in Surf1$^{-/-}$; 2.2 in *Surf1*$^{-/-}$*/PGC-1α*. (2) COX1, 1.8 in *MCK-PGC-1α*; 0.2 in *Surf1*$^{-/-}$; 1.0 in *Surf1*$^{-/-}$*/PGC-1α*. (3) COX5a, 5.0 in *MCK-PGC-1α*; ~0.0 in *Surf1*$^{-/-}$; 1.0 in *Surf1*$^{-/-}$*/PGC-1α*.

(B) MtDNA analysis in different genotypes (three animals/genotype). Color code is as in (A). MtDNA is expressed as number of DNA molecules per cell (Cree et al., 2008). Error bars represent SD.

(C) MRC activities in the different genotypes (three animals/genotype), expressed as nmoles/min/mg of protein. Note that the activity of cII has been multiplied by 10 for visualization clarity. Color code is as in (A). CS, citrate synthase; CI-IV, MRC complexes I–IV. Error bars represent the standard deviation (SD). The asterisks represent the significance levels calculated by unpaired, Student's two-tailed t test: *$p < 0.05$; **$p < 0.01$; ***$p < 0.001$.

(D) Expression analysis of FAO- and OXPHOS-related genes in WT, *Surf1*$^{-/-}$, *MCK-PGC-1α*, *MCK-PGC-1α/Surf1*$^{-/-}$ muscles of mice. The levels of the gene transcripts, retrotranscribed into cDNA, were normalized to that of the *Hprt* gene transcript and expressed as time-fold variation relative to the WT. Error bars represent SD. The asterisks represent the significance levels calculated by unpaired, Student's two-tailed t test: *$p < 0.05$; **$p < 0.01$; ***$p < 0.001$.

(E) COX staining in muscles from different mouse lines including wild-type (WT), *Surf1*$^{-/-}$, *MCK-PGC1α*, and *MCK-PGC1α/Surf1*$^{-/-}$ individuals. Note that the reaction is increased in the *PGC1α* overexpressing mouse models compared to the corresponding naive models. Scale bar, 25 μm, magnification 20×.

In order to test whether *PGC-1α* overexpression may correct specific MRC defects in vivo, we then carried out suitable crosses that transferred the *MCK-PGC-1α* allele into a COX-defective model due to the constitutive ablation of *Surf1*. Surf1 is a putative assembly factor specific to COX, its absence being associated with profound COX deficiency in humans (≤10%–15% of the lower normal limit in different cell types) and, albeit milder, in mice as well (typically 30%–40% of the lower normal limit). While the loss of Surf1 causes early onset, invariably fatal Leigh encephalopathy in patients, recombinant *null* mice showed hardly any clinically deleterious consequence, and standard treadmill test showed no locomotor impairment.

The skeletal muscle of *Surf1*$^{-/-}$*/MCK-PGC-1α* double mutant mice did show the same effects detected in *MCK-PGC-1α* transgenic muscles: increased mtDNA content (from 2078 ± 693 to 4079 ± 824 copies/cell) and CS activity (from 343 ± 33 to 934 ± 226 nmol/min/mg) (Figures 1B and 1C), increased levels of *CD36/FAT* transcript, and increased levels of COX-specific mRNA and protein subunits (Figures 1A and 1D). These changes resulted in (1) partial but significant recovery of COX specific activity (1.6-fold, from 104 ± 24 to 162 ± 42 nmol/min/mg; $p = 0.02$) (Figure 1C), which nevertheless remained well below the normal range (370 ± 49 nmol/min/mg); and (2) increased histochemical reaction to COX (Figure 1E). Taken together, these data suggest that overexpression of *PGC-1α* induces mitochondrial biogenesis and can partially correct a specific defect of COX in vivo.

## Bezafibrate Induces Expression of FAO- but Not OXPHOS-Related Genes

In a second set of experiments, we then tested the effects of PPAR activation in the *Surf1*$^{-/-}$ mouse model. To this end, the same genes, proteins, and activities measured in the *MCK-PGC-1α* and *Surf1*$^{-/-}$*/MCK-PGC-1α* mouse models were also measured in *Surf1*$^{-/-}$ and WT littermates exposed to 0.5% bezafibrate, mixed in standard food for 1 month (Wenz et al., 2008). We observed significant body weight loss during the treatment and marked hepatomegaly at the end of treatment, in both *Surf1*$^{-/-}$ and WT animals (see Figure S1 available online), indicating toxicity of this drug in mice. As expected, the expression of PPAR β/δ and PPAR α, the two PPAR isoforms present in skeletal muscle, was significantly increased in treated animals, along with FAO-related genes, including *CD36/FAT*, *ACOX*, encoding acylCoA oxidase, and *SCAD*, encoding short-chain acylCoA dehydrogenase (Figure 2A). Taken together, these data clearly demonstrated that bezafibrate treatment was indeed effective on the main targets specific for this drug in vivo. Contrariwise, no significant change in mtDNA content, CS, and MRC activities was measured in treated versus untreated *Surf1*$^{-/-}$ or WT muscles (Figures 2B and 2C), and the histochemical reaction to COX was equally defective in both treated and untreated *Surf1*$^{-/-}$ specimens (Figure 2D). Accordingly, the expression of *PGC-1α*, both *NRFs*, and *Tfam* remained unchanged among the different groups of animals, as did several COX subunit transcripts,

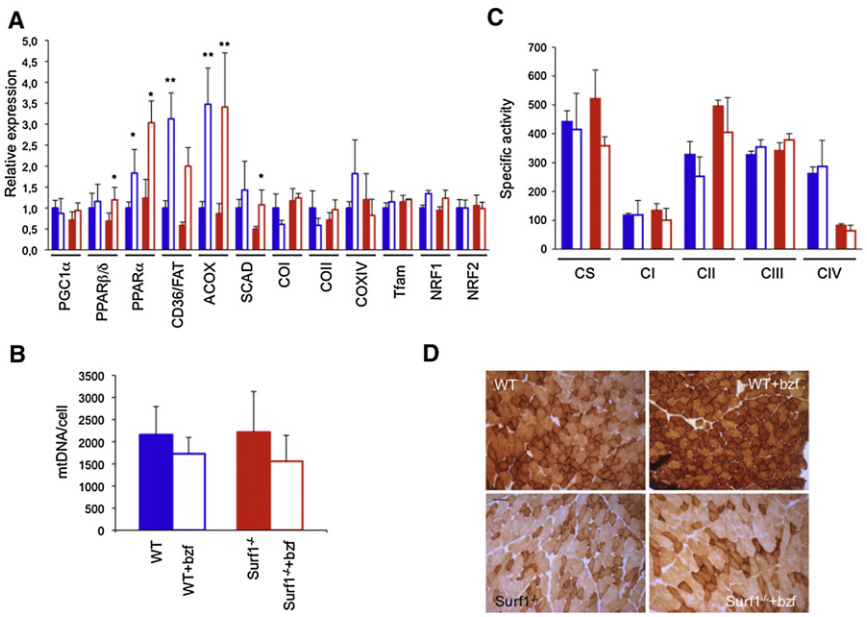


**Figure 2. Bezafibrate Treatment on the *Surf1*$^{-/-}$ Mouse Model**

(A) Expression analysis of FAO- and OXPHOS-related genes in *Surf1*$^{-/-}$ and WT muscles of bezafibrate (bzf)-treated and untreated mice. Solid blue, WT, untreated; blue outline, bzf-treated WT; solid red, *Surf1*$^{-/-}$, untreated; red outline, bzf-treated *Surf1*$^{-/-}$. The levels of the gene transcripts, retrotranscribed into cDNA, were normalized to that of the *Hprt* gene transcript and expressed as time-fold variation relative to the WT. Error bars represent SD. The asterisks represent the significance levels calculated by unpaired, Student's two-tailed t test: *$p < 0.05$; **$p < 0.01$.

(B) MtDNA content analysis in the different genotypes. The color codes are as in (A). Error bars represent SD. MtDNA is expressed as number of DNA molecules per cell (Cree et al., 2008).

(C) MRC activities in the different genotypes, expressed as nmoles/min/mg of protein. Note that the activity of cII has been multiplied by 10 for visualization clarity. Color code is as in (A).

(D) COX staining in muscles from *Surf1*$^{-/-}$ and WT muscles of bzf-treated and untreated mice. Scale bar, 25 μm, magnification 20×.

from either nuclear (e.g., *COXIV*) or mtDNA (*COI* and *COII*) genes (Figure 2A).

## A Muscle-Specific *Cox15* KO Mouse Displays COX-Defective Mitochondrial Myopathy

Since our results failed to confirm those on bezafibrate treatment reported in the *MLC1F-Cox10*$^{-/-}$ mouse model (Wenz et al., 2008), we created a KO mouse for the *Cox15* gene, using the *cre*-lox technology (Figures S2A and S2B). The *Cox15* gene product is the enzyme that comes next to Cox10 in the biosynthetic pathway of *heme a*, the COX-specific *heme* moiety. Cox10 adds a farnesyl chain to *heme b*, converting it into *heme o*, which can then be inserted into the protein backbone of nascent COX. Cox15 eventually converts *heme o* into functionally active *heme a* by oxidation of the $C_8$-methyl group (Khalimonchuk and Rödel, 2005). The constitutive *Cox15*$^{-/-}$ animals, obtained by crossing *Cox15*$^{loxP/loxP}$ mice with a general *cre*-deleter transgenic mouse, showed consistent embryonic lethality at ≤7.5 dpc (not shown). We then produced a muscle-specific *Cox15*$^{-/-}$ model by crossing *Cox15*$^{loxP/loxP}$ with a transgenic mouse expressing the *cre* recombinase under the control of the human skeletal muscle-specific α-actin (ACTA1) promoter (*ACTA-Cox15*$^{-/-}$ mouse).

Recombination of the *Cox15* locus by the *cre* recombinase was detected only in skeletal muscle and, in trace amount, in the heart, whereas no recombination occurs in other tissues (Figure S2C). Accordingly, the amount of *Cox15* mRNA in *ACTA-Cox15*$^{-/-}$ mouse skeletal muscle was ≤16% than that of WT muscle (Figure 3A), and so was the COX/CS ratio (0.05 ± 0.02 in *ACTA-Cox15*$^{-/-}$ versus 0.66 ± 0.06 in WT), whereas there was no significant difference in other tissues (Figure 3B). Albeit born at the expected mendelian ratio, the *ACTA-Cox15*$^{-/-}$ mice were smaller than WT littermates at 30 days after birth (data not shown) and had significantly reduced motor performance measured by a standard treadmill test, initially administered to 4-week-old individuals, and then repeated at 6, 8, 12, and 16 weeks (Figure 3C). Histochemical analysis in skeletal muscle confirmed severe reduction of COX and compensatory proliferation of aberrant mitochondria (Figure 3D), which was confirmed by increased mtDNA content (Figure 3E), increased cII and CS activities (Table S1), and increased SDH histochemical reaction (data not shown), in *ACTA-Cox15*$^{-/-}$ muscles. COX histochemistry was normal in other tissues (data not shown). Except for cII activity, which increased from 24.2 ± 4.2 in WT to 34.9 ± 7.8 in *ACTA-Cox15*$^{-/-}$ muscle homogenate, other MRC activities, including cI and cIII, in muscle (Table S1), and all the MRC activities in nonmuscle tissues (data not shown), of *ACTA-Cox15*$^{-/-}$ were comparable to those of WT littermates.

## Bezafibrate Is Highly Toxic to *ACTA-Cox15*$^{-/-}$ Mice

We then tested the response of eight *ACTA-Cox15*$^{-/-}$ female mice to bezafibrate, according to the same protocol used on the *Surf1*$^{-/-}$ and *MLC1F-Cox10*$^{-/-}$ models. However, after 24–48 hr from the treatment start, the *ACTA-Cox15*$^{-/-}$ animals became critically ill, prompting us to euthanize them. We found worsening of the mitochondrial myopathy (Figures S3A and S3B), and massive apoptosis, demonstrated by numerous TUNEL-positive nuclei (Figures S3C and S3D), corresponding ultrastructurally to chromatin condensation and apoptotic bodies (Figures S3E and S3F). No increased levels of plasma creatine kinase, urea, creatinine, or lactate were detected in plasma of euthanized animals, as observed in massive rhabdomyolysis and acute kidney failure, an adverse effect occasionally reported in patients under bezafibrate treatment (Charach et al., 2005; Wu et al., 2009).

## AICAR Induces FAO and OXPHOS Genes in *Surf1*$^{-/-}$, *Sco2*$^{KO/KI}$, and *ACTA-Cox15*$^{-/-}$ Muscle

In a third set of experiments, we tested the capacity of AICAR, an AMPK agonist, to activate PGC-1α in our animal models. AICAR was given for 1 month in daily subcutaneous injections of

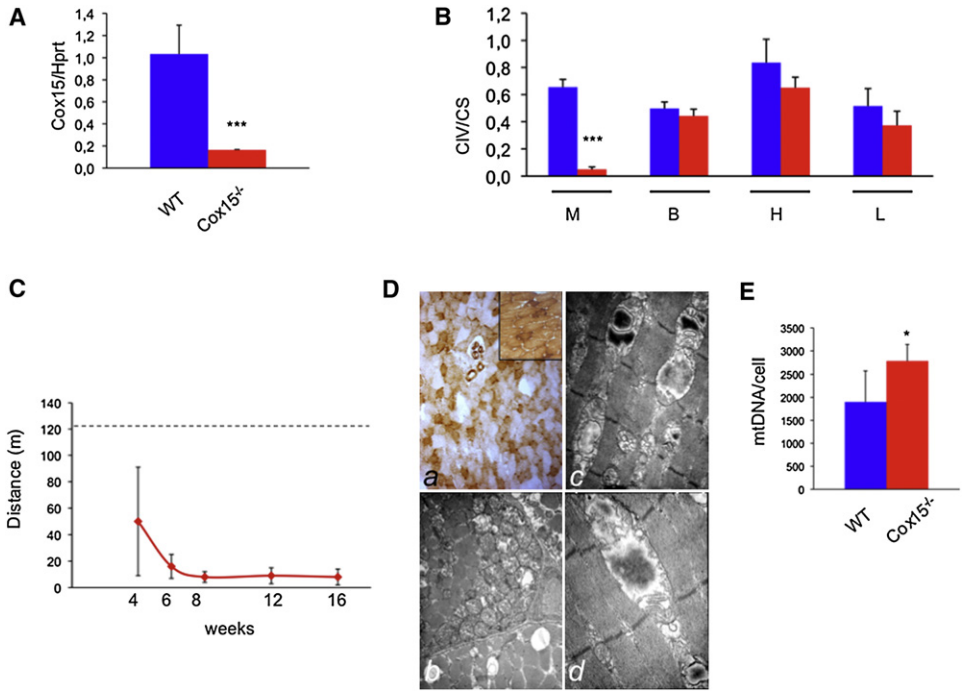


**Figure 3. Characterization of the *ACTA-Cox15*$^{-/-}$ Mouse Model**

(A) *Cox15* transcript levels in skeletal muscle. The *Cox15*-specific mRNA content is ~15% in *ACTA-Cox15*$^{-/-}$ relative to the parental *Cox15*$^{lox/lox}$ mouse line, considered as wild-type (WT). The levels of the *Cox15* gene transcripts, retrotranscribed into cDNA, were normalized to that of the *Hprt* gene transcript and expressed as time-fold variation relative to the WT. Three animals were used for each genotype. Error bars represent SD. The asterisks represent the significance levels calculated by unpaired, Student's two-tailed t test: ***$p < 0.001$.

(B) COX (CIV)-specific activity normalized to that of citrate synthase (CS) in tissues from *ACTA-Cox15*$^{-/-}$ mice. M, muscle; B, brain; H, heart; L, liver. Error bars represent SD. The asterisks represent the significance levels calculated by unpaired, Student's two-tailed t test, ***$p < 0.001$.

(C) Treadmill analysis of *ACTA-Cox15*$^{-/-}$ mice at different time points. The dotted line indicates the lower limit of the motor performance of the parental *Cox15*$^{lox/lox}$ mouse line, considered as WT. Note the rapidly progressive reduction of motor endurance in the *ACTA-Cox15*$^{-/-}$ mouse line over time. Six animals were used for each genotype. Error bars represent SD.

(D) (Top) COX staining from *ACTA-Cox15*$^{-/-}$ skeletal muscle. The inset shows the reaction in a *Cox15*$^{lox/lox}$ (WT) muscle, for comparison. Magnification, 20×. (Bottom) Electron microscopy analysis of *ACTA-Cox15*$^{-/-}$ skeletal muscle. Note the subsarcolemmal accumulation of mitochondria in (Db) (magnification, 7000×) and the presence of an abnormal mitochondria characterized by disruption of the inner membrane and accumulation of electron dense material in (Dc) and (Dd) (magnification, 16,000× and 20,000×, respectively).

(E) MtDNA content in *Cox15*$^{lox/lox}$ (WT) and *ACTA-Cox15*$^{-/-}$ skeletal muscles. Error bars represent SD. The asterisk represents the significance levels calculated by unpaired, Student's two-tailed t test, *$p < 0.05$.

0.25 mg/day/gm of body weight to 2-month-old *Surf1*$^{-/-}$, *Sco2*$^{KO/KI}$, and WT littermates, and of 0.5 mg/day/gm to 2-month-old *ACTA-Cox15*$^{-/-}$ animals and WT littermates, each group being composed of three/four individuals (see legends of Figures 4–6 for details). At the end of treatment, the mtDNA content (data not shown) and CS activity in skeletal muscle (Table S2) were similar in each treated group versus the corresponding untreated group. Analysis of selected transcripts (Figures 4A, 5A, and 6A) showed that, similar to the *MCK-PGC-1α* overexpressing mice, *Nrf1* and *Nrf2* gene expression was unchanged in all groups; however, both *Tfam* and the COX subunit encoding genes were significantly increased in treated versus untreated *Surf1*$^{-/-}$ ($p < 0.05$), *Sco2*$^{KO/KI}$ ($p < 0.01$), and *ACTA-Cox15*$^{-/-}$ muscles ($p < 0.01$). Increased expression of these genes was observed in treated WT mice exposed to the higher (0.5 mg/gm) but not to the lower (0.25 mg/gm) dosage ($p < 0.01$). The expression of the FAO-related *CD36/FAT* gene was significantly increased in all treated groups. *PDK4* and *UCP3*, two genes that are activated by AMPK independently from PGC-1α, were also increased under AICAR treatment. Immunovisualization of selected proteins (Figures 4B, 5B, and 6B) showed that increased expression of COX subunit genes was paralleled by increased amount of COX1 and COX5a proteins in treated *Surf1*$^{-/-}$, *Sco2*$^{KO/KI}$, and *ACTA-Cox15*$^{-/-}$ mice, resulting in significantly increased COX-specific activity (Figures 4C, 5C, and 6C and Tables S2–S4; $p < 0.01$). We also immunovisualized $T_{172}$-phosphorylated (AMPK-P$^{T172}$) versus total muscle AMPK (Figures 4B, 5B, and 6B). Interestingly, the levels of AMPK-P$^{T172}$ were already 8-fold higher in untreated *Surf1*$^{-/-}$ than in untreated WT mice, whereas total AMPK was unchanged. A similar result was obtained in the untreated *ACTA-Cox15*$^{-/-}$ and, albeit less pronounced, in *Sco2*$^{KO/KI}$ muscles. AICAR further increased AMPK phosphorylation in all three COX-defective models, and in WT littermates as well. The quantitative biochemical results obtained by spectrophotometric assays (Figures 4C, 5C, and 6C and Tables S2, S3, and S4) were paralleled by a similar, albeit merely qualitative, trend shown by histochemical reactions to COX (Figures 4D,

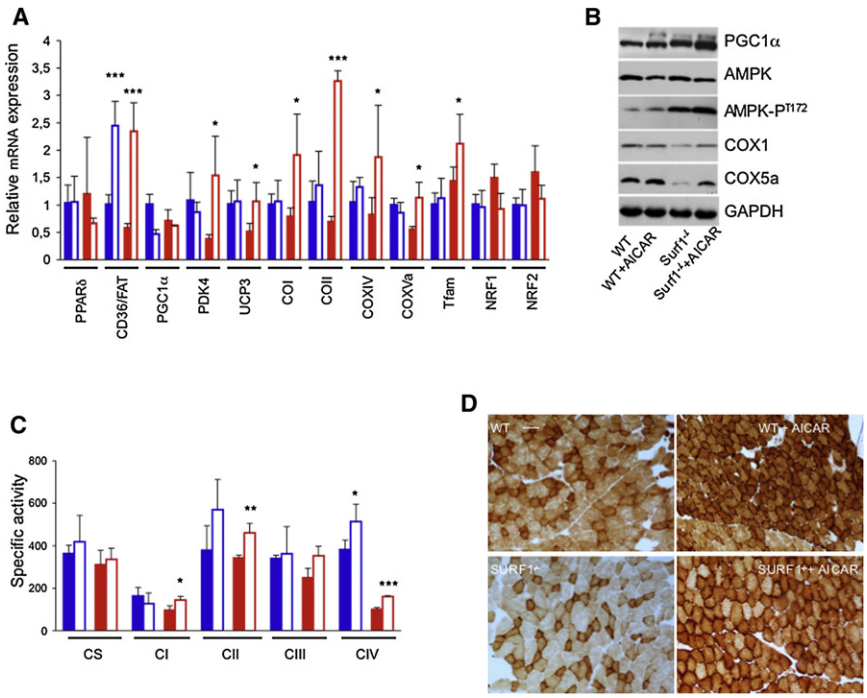


**Figure 4. AICAR Treatment in *Surf1*$^{-/-}$ Mice**

(A) Expression analysis of FAO- and OXPHOS-related genes in *Surf1*$^{-/-}$ and WT muscles of AICAR-treated (0.25 mg/day/gm) and untreated mice. Solid blue, WT, untreated; blue outline, AICAR-treated WT; solid red, *Surf1*$^{-/-}$, untreated; red outline, AICAR-treated *Surf1*$^{-/-}$. The levels of the gene transcripts, retrotranscribed into cDNA, were normalized to that of the *Hprt* gene transcript and expressed as time-fold variation relative to the WT. Error bars represent SD. The asterisks represent the significance levels calculated by unpaired, Student's two-tailed t test: *p < 0.05; **p < 0.01; ***p < 0.001.

(B) Western blot immunovisualization of skeletal muscle proteins of the different genotypes, listed as above. Densitometric analysis of each band, normalized against that of GAPDH, revealed the following variations, relative to untreated WT. (1) PGC-1α: 1.1 in WT+AICAR; 1.5 in *Surf1*$^{-/-}$; 1.8 in *Surf1*$^{-/-}$+AICAR. (2) Total AMPK: 0.8 in WT+AICAR; 1.0 in *Surf1*$^{-/-}$; 0.9 in *Surf1*$^{-/-}$+AICAR. (3) AMPK-P$^{T172}$: 2.3 in WT+AICAR; 8.2 in Surf1$^{-/-}$; 9.5 in *Surf1*$^{-/-}$+AICAR. COX1: 1.0 in WT+AICAR; 0.2 in Surf1$^{-/-}$; 0.6 in Surf1$^{-/-}$+AICAR. (4) COX5a: 1.1 in WT+AICAR; 0.04 in Surf1$^{-/-}$; 0.6 in Surf1$^{-/-}$+AICAR.

(C) MRC activities in the different genotypes, AICAR-treated or untreated, expressed as nmoles/min/mg of protein. Note that the activity of cII has been multiplied by 10 for visualization clarity. Error bars represent SD.

(D) COX staining in skeletal muscles from AICAR-treated and untreated *Surf1*$^{-/-}$ and WT littermates. Note the increased staining of the *Surf1*$^{-/-}$+AICAR sample. Magnification, 20×.

5D, and 6D), SDH (Figures 5D and 6D), and, in treated *ACTA-Cox15*$^{-/-}$ mice, by marked decrease of ultrastructural abnormalities in mitochondria (Figure 6D). Taken together, these results indicate a compensatory activation of the AMPK-Pgc1α axis in conditions of defective COX activity.

## Effect of AICAR Treatment on Motor Performance

In order to evaluate the clinical effect of treatment, we administered a standard, quantitative incremental motor endurance test using a treadmill device. The motor performance was similar to WT littermates in untreated *Surf1*$^{-/-}$ mice, significantly impaired in *Sco2*$^{KO/KI}$ mice, and extremely impaired in *ACTA-Cox15*$^{-/-}$ mice, which were able to walk on the treadmill for just a couple of minutes (Figure 7A). Since no motor phenotype was detected in *Surf1*$^{-/-}$ mice, we focused our analysis on the other two COX-defective models that did show motor impairment. In treated *Sco2*$^{KO/KI}$ mice, the biochemical improvement was mirrored by marked amelioration of motor performance, which reached the same score as the untrained WT littermates by the first to second week of treatment (Figure 7B). Contrariwise, and in spite of partial biochemical recovery, we found no change by treadmill test in *ACTA-Cox15*$^{-/-}$ mice, suggesting that the mitochondrial myopathy was too severe for AICAR treatment to achieve a clinically detectable effect (Figure 7C).

## DISCUSSION

There is no effective treatment for mitochondrial disorders, and current clinical management is focused on treating complications. Stimulation of mitochondriogenesis and MRC activity is one of the strategies that have been proposed to correct OXPHOS failure leading to these conditions.

Two principal systems, PGC-1α and PPARs, are known to increase mitochondrial aerobic metabolism, acting on different, albeit partially overlapping, sets of genes related to mitochondrial bioenergetic pathways.

PGC-1α functions as a coactivator, i.e., it interacts with a number of transcription factors, potentiating their induction of mitochondrial bioenergetics-related genes, including those of OXPHOS. The mechanisms that regulate the expression and activity of PGC-1α are only partially known, but an important role is certainly played by posttranslational modifications of this protein, such as deacetylation, mediated by Sirt1, and phosphorylation, mediated by AMPK.

The control on energy metabolism by PPARs is centered on the activation of mitochondrial FAO, which in turn feeds both the tricarboxylic acids cycle and the MRC. While PPARs are clearly induced by activation of PGC-1α, the opposite effect, i.e., PPAR-dependent induction of PGC-1α, is questioned. In principle, the activation of Sirt1 by $NAD^+$, produced by FAO, links the PPARs system to mitochondriogenesis and OXPHOS, activated by PGC-1α. Another possible mechanism is the direct PPAR-dependent induction of *PGC-1α* mediated by a PPAR-responsive element present in the promoter region of the *PGC-1α* gene. While the latter mechanism has been shown to be active in vitro, several reports have failed to demonstrate a physiologically effective PPAR-dependent control on *PGC-1α* expression and activity in mammalian organisms (Luquet et al., 2003; Wang et al., 2004; Kleiner et al., 2009). However, these mechanisms have been proposed to explain

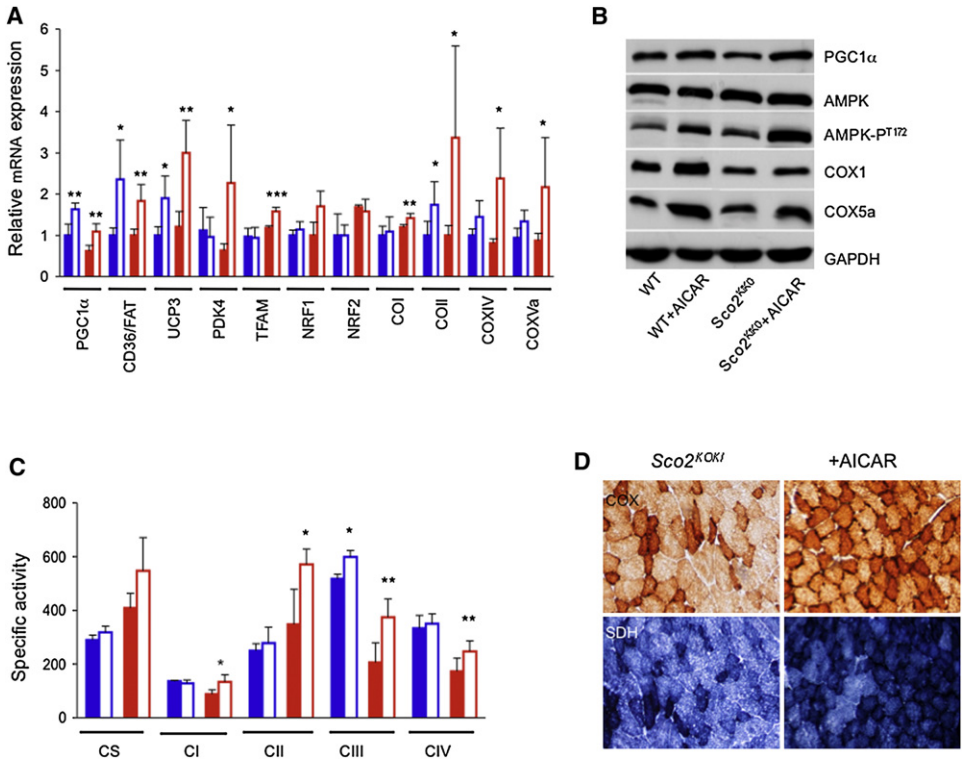


**Figure 5. AICAR Treatment in *Sco2*$^{KO/KI}$ Mice**

(A) Expression analysis of FAO- and OXPHOS-related genes in *Sco2*$^{KO/KI}$ and WT muscles of AICAR-treated (0.25 mg/day/gm) and untreated mice. Solid blue, WT, untreated; blue outline, AICAR-treated WT; solid red, *Sco2*$^{KO/KI}$, untreated; red outline, AICAR-treated *Sco2*$^{KO/KI}$. The levels of the gene transcripts, retrotranscribed into cDNA, were normalized to that of the *Hprt* gene transcript and expressed as time-fold variation relative to the WT. Error bars represent SD. The asterisks represent the significance levels calculated by unpaired, Student's two-tailed t test: *p < 0.05; **p < 0.01; ***p < 0.001.

(B) Western blot immunovisualization of skeletal muscle proteins of the different genotypes, listed as above. Densitometric analysis of each band, normalized against that of GAPDH, revealed the following variations, relative to untreated WT. (1) PGC-1α: 1.7 in WT+AICAR; 1.0 in *Sco2*$^{KO/KI}$; 1.7 in *Sco2*$^{KO/KI}$+AICAR. (2) Total AMPK: 1.0 in WT+AICAR; 1.2 in *Sco2*$^{KO/KI}$; 1.2 in *Sco2*$^{KO/KI}$+AICAR. (3) AMPK-P$^{T172}$: 1.8 in WT+AICAR; 1.6 in *Sco2*$^{KO/KI}$; 3.2 in *Sco2*$^{KO/KI}$+AICAR. COX1: 1.1 in WT+AICAR; 0.6 in *Sco2*$^{KO/KI}$; 0.8 in *Sco2*$^{KO/KI}$+AICAR. (4) COX5a: 1.0 in WT+AICAR; 0.5 in *Sco2*$^{KO/KI}$; 0.7 in *Sco2*$^{KO/KI}$+AICAR.

(C) MRC-specific activities in the different genotypes, AICAR-treated or untreated, expressed as nmoles/min/mg of protein. Note that the activity of cII has been multiplied by 10 for visualization clarity. Error bars represent SD.

(D) COX and SDH staining in skeletal muscles from AICAR-treated and untreated *Sco2*$^{KO/KI}$ and WT littermates. Note the increased staining of the *Sco2*$^{KO/KI}$+AICAR sample. Magnification, 20×.

the recent observation that a pan-PPAR agonist, bezafibrate, was able to correct the COX defect, ameliorate motor impairment, and prolong life span, in *MLC1F-Cox10*$^{-/-}$, a mouse model characterized by muscle-selective ablation of Cox10, a *heme a* biosynthetic enzyme.

To confirm and extend these observations in vivo, we first sought for a proof-of-principle demonstration by showing that (1) marked overexpression of transgenic *Pgc1α* increases the mtDNA content (Lin et al., 2002) and activities of the MRC complexes (this paper) on a WT background; and (2) is also able to partially, albeit not completely, correct COX deficiency in the skeletal muscle of a mildly COX-defective mammalian model, i.e., a constitutive *Surf1*$^{-/-}$ recombinant mouse. These data are largely concordant with results previously obtained in the *MLC1F-Cox10*$^{-/-}$ mouse, and indicate that vigorous stimulation of the Pgc1α axis is effective in increasing OXPHOS in normal and disease conditions in vivo.

Next, we tested the effects of the pharmacological activation of either PPARs- or PGC-1α-regulatory systems in our mouse models. Although these models differ in the severity of biochemical impairment and clinical outcome, all maintain some residual COX activity in skeletal muscle, similar to the corresponding human conditions. This biochemical "leakiness" occurs by different mechanisms in the different mutant organisms. For instance, the function of Surf1 is known to be partially redundant in humans (Tiranti et al., 1999), and even more so in mice (Dell'Agnello et al., 2007). Likewise, while the complete ablation of *Sco2* leads to embryonic lethality (Yang et al., 2010), the combination of a null allele with an allele carrying a missense mutation prevents the activity of the Sco2 protein from being completely abolished. In turn, the excision of *Cox15* in the *ACTA-Cox15*$^{-/-}$ mouse affects a high percentage but not all the muscle fibers, therefore allowing a residual Cox15 activity to be maintained; and all of the reported *SCO2* and *COX15* mutant patients carried missense changes that do not disrupt the corresponding proteins and, presumably, determine a decrease but not the complete loss of their activity. Therefore, all mouse models used in this work carry "permissive" defects that are

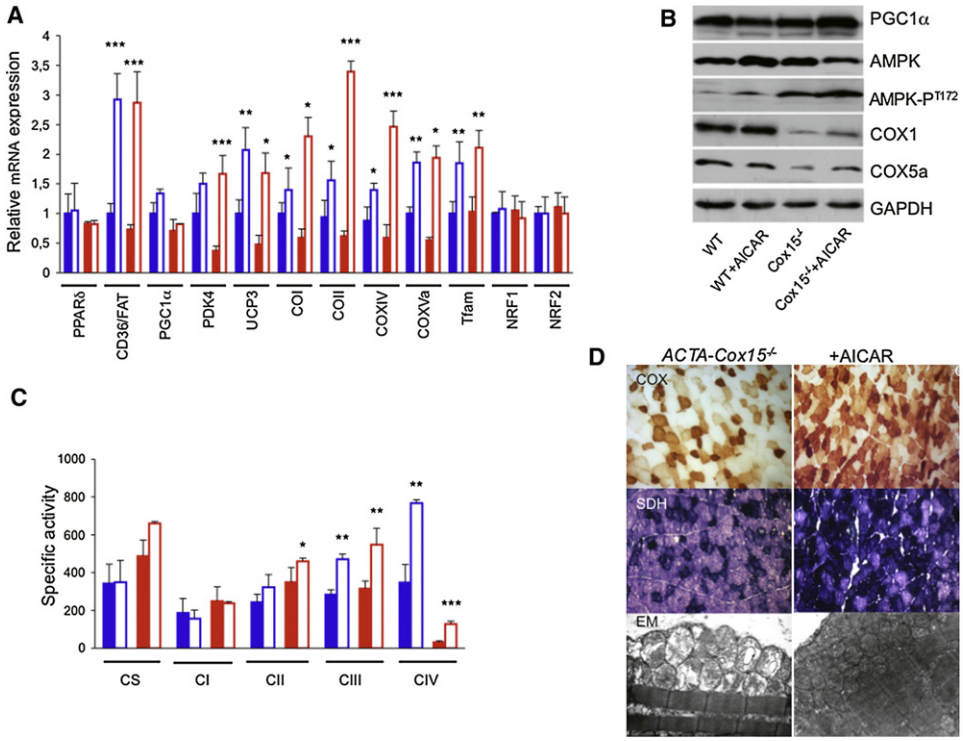


**Figure 6. AICAR Treatment in *ACTA-Cox15*$^{-/-}$ Mice**

(A) Expression analysis of FAO- and OXPHOS-related genes in *ACTA-Cox15*$^{-/-}$ and WT muscles of AICAR-treated (0.5 mg/day/gm) and untreated mice. Solid blue, WT, untreated; blue outline, AICAR-treated WT; solid red, *ACTA-Cox15*$^{-/-}$, untreated; red outline, AICAR-treated *ACTA-Cox15*$^{-/-}$. The levels of the gene transcripts, retrotranscribed into cDNA, were normalized to that of the *Hprt* gene transcript and expressed as time-fold variation relative to the WT. Error bars represent SD. The asterisks represent the significance levels calculated by unpaired, Student's two-tailed t test: *$p < 0.05$; **$p < 0.01$; ***$p < 0.001$.

(B) Western blot immunovisualization of skeletal muscle proteins of the different genotypes, listed as above. Densitometric analysis of each band, normalized against that of GAPDH, revealed the following variations, relative to untreated WT. (1) PGC-1α: 0.9 in WT+AICAR; 1.0 in *ACTA-Cox15*$^{-/-}$; 1.8 in *ACTA-Cox15*$^{-/-}$+AICAR. (2) Total AMPK: 1.8 in WT+AICAR; 1.2 in *ACTA-Cox15*$^{-/-}$; 1.0 in *ACTA-Cox15*$^{-/-}$+AICAR. (3) AMPK-P$^{T172}$: 4 in WT+AICAR; 11.0 in *ACTA-Cox15*$^{-/-}$; 18.0 in *ACTA-Cox15*$^{-/-}$+AICAR. COX1: 1.1 in WT+AICAR; 0.06 in *ACTA-Cox15*$^{-/-}$; 0.4 in *ACTA-Cox15*$^{-/-}$+AICAR. (4) COX5a: 1.0 in WT+AICAR; ~0.1 in *ACTA-Cox15*$^{-/-}$; 0.6 in *ACTA-Cox15*$^{-/-}$+AICAR.

(C) MRC-specific activities in the different genotypes, AICAR-treated or untreated, expressed as nmoles/min/mg of protein. Note that the activity of cII has been multiplied by 10 for visualization clarity. Error bars represent SD.

(D) COX (upper panel) and SDH (middle panel) staining in AICAR-treated and untreated *ACTA-Cox15*$^{-/-}$ and WT muscle. Magnification, 20×. Note the increased staining of the *ACTA-Cox15*$^{-/-}$+AICAR sections. (Bottom) EM of muscles from untreated and AICAR-treated muscles. Note the reduction of abnormal mitochondria in the AICAR-treated mouse.

in principle liable to (partial) correction by stimulating COX biogenesis.

We first stimulated the PPAR axis using bezafibrate, a pan-PPAR agonist, in two COX-defective models: *Surf1*$^{-/-}$, associated with mild COX deficiency and no clinical phenotype, and *ACTA-Cox15*$^{-/-}$, associated with profound COX deficiency and severe mitochondrial myopathy. In spite of the fact that FAO-related genes were in fact induced in treated animals, thus demonstrating that bezafibrate was pharmacologically active, we found neither stimulation of mitochondriogenesis nor induction of MRC enzyme activities, in both *Surf1*$^{-/-}$ and WT animals, which developed instead marked hepatomegaly and body weight loss. The toxic effects of bezafibrate were even more dramatic and rapid in the *ACTA-Cox15*$^{-/-}$ mouse model. Albeit still unknown, the mechanism of the bezafibrate-associated toxicity must be related to the muscle-specific ablation of *Cox15*, and is possibly linked to the very severe COX deficiency present in the skeletal muscle of these animals, since we showed that bezafibrate did not interfere with the maintenance of the gene in extramuscular tissues of the *ACTA-Cox15*$^{-/-}$ model (data not shown). Albeit less dramatic than the toxic myopathy observed in the *ACTA-Cox15*$^{-/-}$ model, adverse effects, such as body weight loss and hepatomegaly, were also observed in other bezafibrate-treated animal models, including mice with milder COX deficiency, such as (1) our constitutive *Surf1*$^{-/-}$ mouse model (Figure S1); and (2) the *Sco2*$^{KO/KI}$ mouse (E.A.S., unpublished data); as well as in animals with other OXPHOS defects, such as (3) constitutive *Mpv17*$^{-/-}$ mice (C.V. and M.Z., unpublished data). On a practical side, we believe that these observations in mice should prompt physicians to be cautious on the use of bezafibrate in patients with severe MRC defects, particularly COX deficiencies.

We then activated the PGC-1α axis by treating our mouse models with the AMPK agonist AICAR. Interestingly, we found that the levels of activated AMPK-P$^{172}$ were already higher in skeletal muscle of untreated COX-defective models than in WT

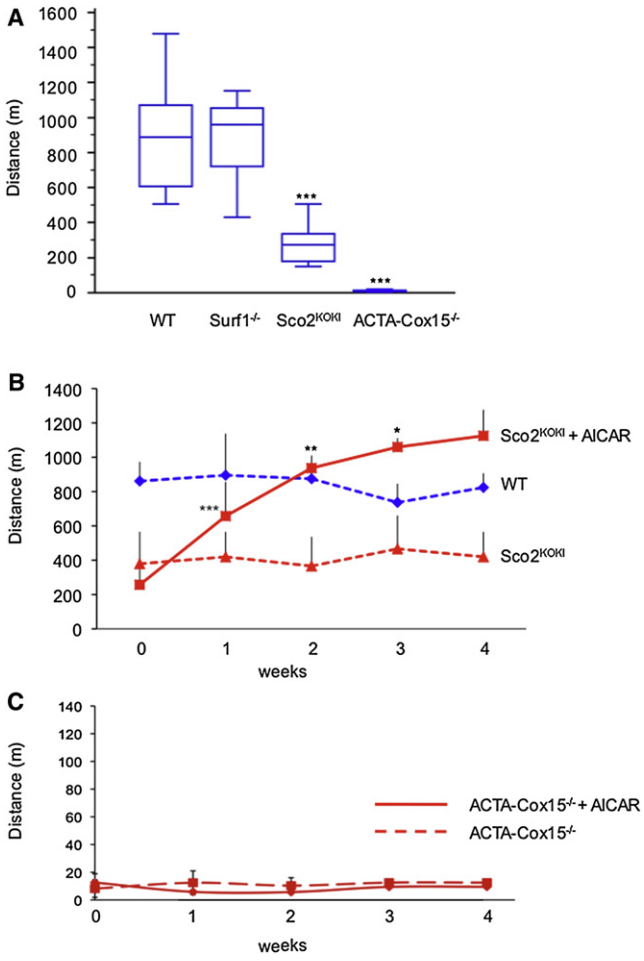


**Figure 7. Treadmill Test**

(A) Box-and-whisker plot of treadmill tests administered to WT (n. 16), *Surf1*$^{-/-}$ (n. 11), *Sco2*$^{KO/KI}$ (n. 9), and *ACTA-Cox15*$^{-/-}$ (n. 11) mice at 3 months of age. There is no motor impairment in *Surf1*$^{-/-}$; significant motor impairment in *Sco2*$^{KO/KI}$ and severe motor impairment in *ACTA-Cox15*$^{-/-}$ mice compared to WT mice. The vertical bars represent the range of values; the boxes represent the values from the lower to upper quartile; the horizontal lines represent the median value for each group of animals. ***, unpaired, Student's two-tailed t test: $p < 10^{-6}$.

(B) Treadmill test in AICAR-treated *Sco2*$^{KO/KI}$ and in untreated *Sco2*$^{KO/KI}$ and WT littermates. Each group was composed of four individuals. The scores of motor performance measured week by week showed significant improvement in the AICAR-treated *Sco2*$^{KO/KI}$ animals during the first 3 weeks of treatment (paired, Student's two-tailed t test ***$p < 0.001$; **$p < 0.01$; *$p < 0.05$), with an additional, albeit not significant, increment at week 4. Notably, the score of the AICAR-treated *Sco2*$^{KO/KI}$ animals became not significantly different from that of untreated WT littermates at the end of the first week, identical to that of WT at the second week, and significantly higher at the third and fourth weeks of treatment. Note that untreated WT or *Sco2*$^{KO/KI}$ mice showed no change in motor performance over time, indicating no significant effect of training. Vertical bars show the SDs.

(C) Treadmill test in untreated and AICAR-treated *ACTA-Cox15*$^{-/-}$ mice. No change was detected in motor performance over time. Vertical bars show the SDs.

controls, and further increased upon AICAR treatment. This finding could be occurring because of the homeostatic loop that relates the PGC-1α axis to the activity of MRC (Wallace and Fan, 2010), and can explain why the response of the latter to AICAR was significantly higher in COX-defective muscles than in WT muscles.

The ~1.5-fold increase of *PGC1α* transcript and AMPK-dependent activation of the corresponding protein induced by AICAR did not determine an increase of the mtDNA content of skeletal muscle, as observed in the *MCK-PGC1α* models, where *PGC1α* is >10-fold expressed compared to WT muscle. This result suggests that the increase of OXPHOS-related proteins and activities, including COX, that was observed in AICAR-treated COX-defective mice, are likely due to increased transcription and translation of the corresponding genes, in agreement with the increased levels of *Tfam* expression. Importantly, the *Sco2*$^{KO/KI}$ mice, which are characterized by mild, but significant, motor impairment, did markedly improve their performance under AICAR treatment, in parallel with recovery of COX activity in skeletal muscle. Unfortunately, no motor impairment was measured in untreated *Surf1*$^{-/-}$ mice (Figure 7A), which prevented us from further investigating the clinical features of this model under AICAR treatment. Contrariwise, the *ACTA-COX15*$^{-/-}$ mouse model showed very severe impairment of motor performance at 2 months of age, which failed to respond to AICAR, in spite of doubling the daily dosage of the drug (0.5 mg/gm versus 0.25 mg/gm). Further dosage increase, earlier and prolonged treatment, and association with other drugs (e.g., antioxidants) are warranted in this model to possibly improve clinical efficacy. Unlike the results obtained with AICAR, bezafibrate had no effect on OXPHOS, whereas it was clearly effective in inducing FAO-related genes. Acute exposure of MRC-defective cultured fibroblasts to high-dose bezafibrate has given controversial results (Bastin et al., 2008): some cell lines did respond by increasing MRC activities, others, including a *Surf1*$^{-/-}$ cell line, did not, which suggests that the responsiveness to the drug may depend on a number of still undisclosed variables, possibly intrinsic to the cell type and culturing conditions. Likewise, we have no obvious explanation for the discrepancy between our results and those recently reported in the *MLC1F-Cox10*$^{-/-}$ mouse model. One possibility is that the *MLC1F-Cox10*$^{-/-}$ model is characterized by predominant excision of the *Cox10* gene in fast-twitch, type 2, glycolytic muscle fibers, whereas the slow-twitch, type 1, oxidative fibers are relatively spared. Therefore, a shift in favor of the latter type induced by bezafibrate-dependent activation of PPARs could explain the improvement in COX activity, exercise performance, and eventually life span of the treated animals. Nevertheless, other effects reported with this model, for instance increased expression of *Pgc1α*, were not observed in ours. One reason may be related to the fact that the PPAR system acts on Pgc1α via FAO induction and stimulation of $NAD^+$-dependent Sirt1 deacetylase (Gerhart-Hines et al., 2007); however, block of mitochondrial respiration, as occurs in COX deficiency, typically decreases the $NAD^+$/NADH ratio and should in fact reduce the activation of Sirt1 (Wallace, 2005), thus opposing the effect of PPAR activation.

Taken together, the results of our study prove that pharmacological activation of mitochondrial biogenesis is a rational, potentially effective approach to mitochondrial disease. Nevertheless, since both AICAR and activated AMPK determine a host of pleiotropic effects on different regulatory and homeostatic pathways

(Cantó et al., 2010), prolonged observation on chronically treated animals is needed to establish treatment safety and eventual translatability to humans.

## EXPERIMENTAL PROCEDURES

### Reagents and Materials

AICAR was from Toronto Research Chemicals. Anti-PGC-1α antibody was from Abcam; anti-AMPK and anti-AMPK-P antibodies were from Cell Signaling; anti-COI and -COX5a were from Invitrogen; anti-GAPDH was from Millipore. Anti-rabbit and anti-mouse secondary antibodies were from Amersham. Chemicals were from Sigma. MCK-PGC-1α and ACTA-Cre transgenic mice were obtained from Jackson Laboratory, Bar Harbor, USA. Oligonucleotides were from PRIMM, Italy. The sequences of all the primers used in this study are available on request.

### Western Blot Analysis

Total homogenates were prepared in RIPA buffer (50 mM Tris HCl [pH 8], 150 mM NaCl, 1% NP-40, 0.5% sodium deoxycholate, 0.1% SDS) with the addition of a protease inhibitor cocktail (Roche). Protein concentration was determined by the Lowry method. Aliquots, 80 μg each, were run through a 12% SDS-PAGE and electroblotted onto a nitrocellulose membrane, which was then matched with different antibodies.

### In Vivo Experiments

Animal studies were in accordance with the Italian Law D.L. 116/1992 and the EU directive 86/609/CEE. Standard food and water were given ad libitum. Mice were maintained in a temperature- and humidity-controlled animal-care facility, with a 12 hr light/dark cycle and free access to water and food (Standard Diet, Mucedola, Italy). Bezafibrate (Sigma) 0.5% was added to a standard diet (Mucedola, Italy) and administered for 1 month. AICAR or vehicle was administered for 4 weeks with a single daily subcutaneous injection. No difference in daily monitored water and food intake was detected between the treated versus untreated groups of animals during the experiment. Animals were sacrificed by cervical dislocation.

### Treadmill Test

A treadmill apparatus (Columbus Instruments, Columbus, OH) was used to measure motor exercise endurance according to the number of falls in the motivational grid during a gradually accelerating program with speed initially at 6.5 m/min and increasing by 0.5 m/min every 3 min. The test was terminated by exhaustion, defined as >10 falls/min into the motivational grid.

### Morphological Analysis

Histochemical and ultrastructural analyses were performed as described (Sciacco and Bonilla, 1996; Dubowitz, 1985). TUNEL reaction was performed following the manufacturer's instructions (In Situ Cell Death Detection Kit, Roche, Germany).

### Biochemical Analysis of MRC Complexes

Muscle quadriceps samples stored in liquid nitrogen were homogenized in 10 mM phosphate buffer (pH 7.4), and the spectrophotometric activity of cI, cII, cIII and cIV, as well as CS, was measured as described (Bugiani et al., 2004).

### Real-Time PCR

For mtDNA content analysis, SYBR Green real-time PCR was performed using primers specific to a mouse mtDNA region in the *COI* gene and primers specific to RNaseP, a single copy gene taken as a nuclear gene reference, as described (Viscomi et al., 2009). For the analysis of transcripts, total RNA was extracted from liquidnitrogen snap frozen muscle by Trizol, according to the manufacturer's instructions (Invitrogen, Carlsbad, CA, USA). Of total RNA, 2 μg was treated with RNase free-DNase and retrotranscribed using the "cDNA cycle" kit (Invitrogen, Carlsbad, CA, USA). Approximately 2–5 ng of cDNA was used for real-time PCR assay using primers specific for amplification of several genes.

### Creation of a Recombinant Cox15 KO Mouse

A mouse genomic region spanning *Cox15* exons 1–2 was PCR amplified with suitable oligos to introduce a *loxP* site, and cloned into a vector containing a Neomycin resistance cassette, flanked by two *Flp* sites, and a second *loxP* site. The short and long arms of homology were amplified by PCR using suitable oligos and cloned into the vector containing the floxed region. The final targeting vector was linearized by digestion with XhoI and electroporated in 129Sv cells. A total of 600 clones were PCR screened by PCR (see legend of Figure S2). In one recombinant clone, homologous recombination was ascertained on the long arm by long-range PCR (see Figure S2). Injection into C57Bl/6 blastocysts was followed by selection of chimaeric individuals, which were then backcrossed to a C57Bl/6 female. The recombinant mice were crossed to a general deleter *cre* transgenic mouse to obtain $Cox15^{+/-}$ heterozygous mice, which were then crossed to a *Flpe* transgenic mouse in order to eliminate the neomycin-resistance cassette, resulting in $Cox15^{lox/lox}$ individuals. *ACTA-*$Cox15^{-/-}$ mice were eventually obtained by crossing $Cox15^{lox/lox}$ with *ACTA-Cre* mice.

## SUPPLEMENTAL INFORMATION

Supplemental Information includes four tables and three figures and can be found with this article online at doi:10.1016/j.cmet.2011.04.011.

## ACKNOWLEDGMENTS

This work was supported by the Pierfranco and Luisa Mariani Foundation Italy; Fondazione Telethon-Italy grants numbers GGP07019 and GPP10005; Fondazione Tomasello and Associazione Mitocon to M.Z.; the National Institutes of Health (grant HD32062), the Muscular Dystrophy Association, and the Marriott Mitochondrial Disorder Clinical Research Fund to E.A.S.; and the "Associazione Amici del Centro Dino Ferrari" to M.M.

Received: January 19, 2011
Revised: March 23, 2011
Accepted: April 8, 2011
Published: July 5, 2011

## REFERENCES

Antonicka, H., Mattman, A., Carlson, C.G., Glerum, D.M., Hoffbuhr, K.C., Leary, S.C., Kennaway, N.G., and Shoubridge, E.A. (2003). Mutations in COX15 produce a defect in the mitochondrial heme biosynthetic pathway, causing early-onset fatal hypertrophic cardiomyopathy. Am. J. Hum. Genet. *72*, 101–114.

Barish, G.D., Narkar, V.A., and Evans, R.M. (2006). PPAR delta: a dagger in the heart of the metabolic syndrome. J. Clin. Invest. *116*, 590–597.

Bastin, J., Aubey, F., Rotig, A., Munnich, A., and Djouadi, F. (2008). Activation of peroxisome proliferator activated receptor pathway stimulates the mitochondrial respiratory chain and can correct deficiencies in patients' cells lacking its components. J. Clin. Endocrinol. Metab. *4*, 1433–1441.

Bugiani, M., Invernizzi, F., Alberio, S., Briem, E., Lamantea, E., Carrara, F., Moroni, I., Farina, L., Spada, M., Donati, M.A., et al. (2004). Clinical and molecular findings in children with complex I deficiency. Biochim. Biophys. Acta *1659*, 136–147.

Bugiani, M., Tiranti, V., Farina, L., Uziel, G., and Zeviani, M. (2005). Novel mutations in COX15 in a long surviving Leigh syndrome patient with cytochrome c oxidase deficiency. J. Med. Genet. *42*, e28. 10.1136/jmg.2004.029926.

Cantó, C., and Auwerx, J. (2010). AMP-activated protein kinase and its downstream transcriptional pathways. Cell. Mol. Life Sci. *67*, 3407–3423.

Cantó, C., Gerhart-Hines, Z., Feige, J.N., Lagouge, M., Noriega, L., Milne, J.C., Elliott, P.J., Puigserver, P., and Auwerx, J. (2009). AMPK regulates energy expenditure by modulating NAD+ metabolism and SIRT1 activity. Nature *458*, 1056–1060.

Charach, G., Grosskopf, I., Rotmensch, H.H., Kitzis, I., and Weintraub, M. (2005). Bezafibrates cause moderate, reversible impairment in renal function in patients without prior renal disease. Nephron Clin. Pract. *100*, c120–c125.

Corton, J.M., Gillespie, J.G., Hawley, S.A., and Hardie, D.G. (1995). 5-amino-imidazole-4-carboxamide ribonucleoside. A specific method for activating AMP-activated protein kinase in intact cells? Eur. J. Biochem. *229*, 558–565.

Cree, L.M., Patel, S.K., Pyle, A., Lynn, S., Turnbull, D.M., Chinnery, P.F., and Walker, M. (2008). Age-related decline in mitochondrial DNA copy number in isolated human pancreatic islets. Diabetologia *51*, 1440–1443.

Dell'Agnello, C., Leo, S., Agostino, A., Szabadkai, G., Tiveron, C., Zulian, A., Prelle, A., Roubertoux, P., Rizzuto, R., and Zeviani, M. (2007). Increased longevity and refractoriness to Ca(2+)-dependent neurodegeneration in Surf1 knockout mice. Hum. Mol. Genet. *16*, 431–444.

Dubowitz, V. (1985). Muscle Biopsy, A Practical Approach, 2nd ed. (London: Baillière Tindall).

Fogarty, S., Hawley, S.A., Green, K.A., Saner, N., Mustard, K.J., and Hardie, D.G. (2010). Calmodulin-dependent protein kinase kinase-β activates AMPK without forming a stable complex: synergistic effects of Ca2+ and AMP. Biochem. J. *426*, 109–118.

Gerhart-Hines, Z., Rodgers, J.T., Bare, O., Lerin, C., Kim, S.H., Mostoslavsky, R., Alt, F.W., Wu, Z., and Puigserver, P. (2007). Metabolic control of muscle mitochondrial function and fatty acid oxidation through SIRT1/PGC-1alpha. EMBO J. *26*, 1913–1923.

Goldman, S.J., Taylor, R., Zhang, Y., and Jin, S. (2010). Autophagy and the degradation of mitochondria. Mitochondrion *10*, 309–315.

Handschin, C., and Spiegelman, B.M. (2006). Peroxisome proliferator-activated receptor gamma coactivator 1 coactivators, energy homeostasis, and metabolism. Endocr. Rev. *27*, 728–735.

Jäger, S., Handschin, C., St-Pierre, J., and Spiegelman, B.M. (2007). AMP-activated protein kinase (AMPK) action in skeletal muscle via direct phosphorylation of PGC-1alpha. Proc. Natl. Acad. Sci. USA *104*, 12017–12022.

Kelly, D.P., and Scarpulla, R.C. (2004). Transcriptional regulatory circuits controlling mitochondrial biogenesis and function. Genes Dev. *18*, 357–368.

Khalimonchuk, O., and Rödel, G. (2005). Biogenesis of cytochrome c oxidase. Mitochondrion *5*, 363–388.

Kleiner, S., Nguyen-Tran, V., Baré, O., Huang, X., Spiegelman, B., and Wu, Z. (2009). PPAR{delta} agonism activates fatty acid oxidation via PGC-1{alpha} but does not increase mitochondrial gene expression and function. J. Biol. Chem. *284*, 18624–18633.

Lagouge, M., Argmann, C., Gerhart-Hines, Z., Meziane, H., Lerin, C., Daussin, F., Messadeq, N., Milne, J., Lambert, P., Elliott, P., et al. (2006). Resveratrol improves mitochondrial function and protects against metabolic disease by activating SIRT1 and PGC-1alpha. Cell *127*, 1109–1122.

Leary, S.C., Sasarman, F., Nishimura, T., and Shoubridge, E.A. (2009). Human SCO2 is required for the synthesis of CO II and as a thiol-disulphide oxidoreductase for SCO1. Hum. Mol. Genet. *18*, 2230–2240.

Lefebvre, P., Chinetti, G., Fruchart, J.C., and Staels, B. (2006). Sorting out the roles of PPAR alpha in energy metabolism and vascular homeostasis. J. Clin. Invest. *116*, 571–580.

Lin, J., Wu, H., Tarr, P.T., Zhang, C.-Y., Wu, Z., Boss, O., Michael, L.F., Puigserver, P., Isotani, E., Olson, E.N., et al. (2002). Transcriptional co-activator PGC-1α drives the formation of slow-twitch muscle fibers. Nature *418*, 797–801.

Luquet, S., Lopez-Soriano, J., Holst, D., Fredenrich, A., Melki, J., Rassoulzadegan, M., and Grimaldi, P.A. (2003). Peroxisome proliferator-activated receptor delta controls muscle development and oxidative capability. FASEB J. *17*, 2299–2301.

Merrill, G.F., Kurth, E.J., Hardie, D.G., and Winder, W.W. (1997). AICA riboside increases AMP-activated protein kinase, fatty acid oxidation, and glucose uptake in rat muscle. Am. J. Physiol. *273*, 1107–1112.

Papadopoulou, L.C., Sue, C.M., Davidson, M.M., Tanji, K., Nishino, I., Sadlock, J.E., Krishna, S., Walker, W., Selby, J., Glerum, D.M., et al. (1999). Fatal infantile cardioencephalomyopathy with COX deficiency and mutations in SCO2, a COX assembly gene. Nat. Genet. *23*, 333–337.

Sciacco, M., and Bonilla, E. (1996). Cytochemistry and immunocytochemistry of mitochondria in tissue sections. Methods Enzymol. *264*, 509–521.

Srivastava, S., Diaz, F., Iommarini, L., Aure, K., Lombes, A., and Moraes, C.T. (2009). PGC-1alpha/beta induced expression partially compensates for respiratory chain defects in cells from patients with mitochondrial disorders. Hum. Mol. Genet. *18*, 1805–1812.

Steinberg, G.R., and Kemp, B.E. (2009). AMPK in health and disease. Physiol. Rev. *89*, 1025–1078.

Tenenbaum, A., Motro, M., and Fisman, E.Z. (2005). Dual and pan-peroxisome proliferator-activated receptors (PPAR) co-agonism: the bezafibrate lessons. Cardiovasc. Diabetol. *16*, 4–14.

Tiranti, V., Galimberti, C., Nijtmans, L., Bovolenta, S., Perini, M.P., and Zeviani, M. (1999). Characterization of SURF-1 expression and Surf-1p function in normal and disease conditions. Hum. Mol. Genet. *8*, 2533–2540.

Viscomi, C., Spinazzola, A., Maggioni, M., Fernandez-Vizarra, E., Massa, V., Pagano, C., Vettor, R., Mora, M., and Zeviani, M. (2009). Early-onset liver mtDNA depletion and late-onset proteinuric nephropathy in Mpv17 knockout mice. Hum. Mol. Genet. *18*, 12–26.

Wallace, D.C. (2005). A mitochondrial paradigm of metabolic and degenerative diseases, aging, and cancer: a dawn for evolutionary medicine. Annu. Rev. Genet. *39*, 359–407.

Wallace, D.C. (2010). Mitochondrial energetics and therapeutics. Annu. Rev. Pathol. *5*, 297–348.

Wallace, D.C., and Fan, W. (2010). Energetics, epigenetics, mitochondrial genetics. Mitochondrion *10*, 12–31.

Wang, Y.X., Zhang, C.L., Yu, R.T., Cho, H.K., Nelson, M.C., Bayuga-Ocampo, C.R., Ham, J., Kang, H., and Evans, R.M. (2004). Regulation of muscle fiber type and running endurance by PPARdelta. PLoS Biol. *2*, e294. 10.1371/journal.pbio.0020294.

Wenz, T., Diaz, F., Spiegelman, B.M., and Moraes, C.T. (2008). Activation of the PPAR/PGC-1alpha pathway prevents a bioenergetic deficit and effectively improves a mitochondrial myopathy phenotype. Cell Metab. *8*, 249–256.

Wu, J., Song, Y., Li, H., and Chen, J. (2009). Rhabdomyolysis associated with fibrate therapy: review of 76 published cases and a new case report. Eur. J. Clin. Pharmacol. *65*, 1169–1174.

Yang, H., Brosel, S., Acin-Perez, R., Slavkovich, V., Nishino, I., Khan, R., Goldberg, I.J., Graziano, J., Manfredi, G., and Schon, E.A. (2010). Analysis of mouse models of cytochrome c oxidase deficiency owing to mutations in Sco2. Hum. Mol. Genet. *19*, 170–180.

Zeviani, M., and Di Donato, S. (2004). Mitochondrial disorders. Brain *127*, 2153–2172.